This article has been accepted for publication in a future issue of this journal, but has not been fully edited. Content may change prior to final publication. Citation information: DOI 10.1109/ACCESS.2020.2993806, IEEE Access

IEEE Access
Multidisciplinary ⋮ Rapid Review ⋮ Open Access Journal

Date of publication xxxx 00, 0000, date of current version xxxx 00, 0000.

Digital Object Identifier 10.1109/ACCESS.2017.Doi Number

A Novel Method Simulating Human Eye Recognition for Sector Judgement of SVPWM Algorithm

Qingsong Wang[1, 2], Panhong Chen[1], Fujin Deng[1*], Ming Cheng[1], Giuseppe Buja[3]

[1]School of Electrical Engineering, Southeast University, 210096 Nanjing, China
[2]Jiangsu Key Laboratory of Smart Grid Technology and Equipment, 212000 Zhenjiang, China
[3]Department of Industrial Engineering, University of Padova, 35131 Padova, Italy

Corresponding author: Fujin Deng (email: fdeng@seu.edu.cn).

ABSTRACT The conventional space vector pulse width modulation (SVPWM) algorithm is mature and widely used in the control of three-phase inverters. As we know, the position of the voltage vectors can be seen directly by human eyes, which can be used to replace the existing way for sector selection in the conventional SVPWM algorithm. Based on the fact, a novel method simulating human eye recognition for sector selection of SVPWM is proposed in this paper. In the real application, machine can replace human eyes, and it can 'see' the sector step by step in which the voltage vector is located, and immediately give the switching time of the two non-zero voltage vectors. Theoretically, it can save the running time and complexity of the SVPWM algorithm reflected in the situation that multiple inverters are connected in parallel with the number of voltage vectors being increased. The feasibility of the proposed SVPWM algorithm has been validated by both simulation and experiments, which offers the possibility of the application in the multiple or multilevel converters.

INDEX TERMS SVPWM, machine vision, voltage vector, multiple inverters.

I. INTRODUCTION

SVPWM is a relatively novel control method developed in recent years. It is a pulse width modulated wave generated by a specific switching mode composed of six power switching elements of a three-phase power inverter, which can make the output current waveform as close as possible to an ideal sinusoidal waveform [1]–[2]. Before that, the Sinusoidal Pulse Width Modulation (SPWM) strategy has been widely used in AC variable frequency speed control systems, but the SPWM method cannot fully utilize the DC voltage fed to the inverter [3]. SPWM is based on adjusting the pulse width and spacing to achieve close to sinusoidal output current, which will still produce some higher harmonic components [4], causing motor heating, torque ripple and even system oscillation [5]–[6]. In addition, SPWM is suitable for analog circuits, which is not convenient for digital implementation [7]–[8].

Space Vector PWM (SVPWM) is different from SPWM. It starts from the overall effect of three-phase output voltage and focuses on how to make the motor obtain the ideal circular flux linkage [9]–[10]. Compared with SPWM, the SVPWM technology has a small harmonic component of the winding current waveform, which reduces the torque ripple of the motor, and the rotating magnetic field is closer to a circular shape [11]. Moreover, the utilization of the DC bus voltage is greatly improved, and it is easier to digitize [12]–[13].

In addition to playing an important role in the control of AC motors [14], SVPWM is also used in the control of inverters with the popularization of renewable energy generation [15], for instance, Photovoltaic (PV) system. As the requirements for higher voltage capability and lower harmonic distortion increases, SVPWM offers significant performance benefits in multilevel converters. Multilevel converters have been extensively studied in a wide variety of applications. In [16]–[18], SVPWM algorithm being used in multilevel converters is presented. A novel SVPWM algorithm based on line voltage coordinate is studied in [16] to simplify the steps of determining the basic vectors and the solution about the basic vector corresponding action time. In [17], a new Space Vector Pulse Width Modulation scheme to reconstruct phase

This work is licensed under a Creative Commons Attribution 4.0 License. For more information, see https://creativecommons.org/licenses/by/4.0/.

This article has been accepted for publication in a future issue of this journal, but has not been fully edited. Content may change prior to final publication. Citation information: DOI 10.1109/ACCESS.2020.2993806, IEEE Access

currents is presented, using neutral-point current sensing in three-level T-type converters. Sector determination for a normalised SVPWM scheme is proposed in [18] for four-switch three-phase voltage source inverter by using already available stationary reference frame stator voltages without requiring complex trigonometric calculations.

It is obvious that vector selection is so critical in the SVPWM algorithm. And the complexity of vector diagram increases as the converters become more and more complex. For instance, in the neutral-point clamped (NPC) three-level inverters [19]–[20], hundreds of vectors are used which makes it so complicated. At such situation, traditional way for sector judgement needs to be updated. Fortunately, the vector space diagram could easily be seen and located by human eyes. With the development of digital control, the functionality of human vision can be realized through machine vision. Based on the fact above, this paper proposes a novel method for sector judgement to replace the traditional way. The proposed method is an offline calculation similar to "table lookup", which has more advantages in execution time compared to the conventional method, especially in multi-level inverters.

In detail, this paper is organized as follows. Section II reviews the operating principle of conventional SVPWM. Section III proposes a novel method simulating human eye recognition for sector judgement together with its operating functionalities. Section IV presents simulations and Section V introduces experiments carried out in the lab operated with the proposed control. Finally, Section VI concludes the paper.

II. PRINCIPLES OF CONVENTIONAL SVPWM ALGORITHM

The theoretical basis of SVPWM is the principle of average value equivalence. The circumference of the voltage space vector is uniformly divided into N equal parts. In each switching period designated as T_s, the average value is equal to the reference voltage vector by the combination of basic voltage vectors, where $T_s=(1/f)/N$, f is the fundamental frequency of a given three-phase voltage, typically 50 Hz. The basic voltage vector contains non-zero and zero vectors, and different vectors are determined by the on-and-off conditions of the upper and lower arms of the three-phase inverters. As a result, the entire SVPWM algorithm is generalized to calculate the switching time of non-zero and zero vectors at a predefined voltage vector, and further convert to the switching state and time of the three-phase inverter to control the switches to get the PWM waveform finally.

A. BASIC PRINCIPLE

Assuming that the DC bus voltage is U_{dc}, the three-phase voltage outputs of the inverter are U_A, U_B, and U_C, the phase of which differ by 120° in space and varies in sinusoidal shape over time on their respective axes. The resultant voltage trajectory is a circle that moves uniformly in space. Suppose U_m is the effective value of the phase voltage, f is the fundamental frequency, and then we can get:

$$\begin{cases} U_A(t)=\sqrt{2}U_m\cos(2\pi ft) \\ U_B(t)=\sqrt{2}U_m\cos\left(2\pi ft-\dfrac{2\pi}{3}\right) \\ U_C(t)=\sqrt{2}U_m\cos\left(2\pi ft+\dfrac{2\pi}{3}\right) \end{cases} \tag{1}$$

The combined space vector $U(t)$ can be expressed as:

$$U(t)=\frac{2}{3}\left[U_A(t)+U_B(t)e^{j2\pi/3}+U_C(t)e^{j4\pi/3}\right]=\sqrt{2}U_m e^{j2\pi ft} \tag{2}$$

It is seen from (2) that the three-phase composite voltage is a rotating space vector rotating counterclockwise at an angular velocity $\omega=2\pi f$. Meanwhile, the amplitude is fixed, which is the peak value of the phase voltage, and the projection of $U(t)$ on the three-phase coordinate axis is a symmetric three-phase sinusoidal quantity.

As we know, three-phase inverter has six switches which can be defined as S_x ($x=a, b, c$):

$$S_x=\begin{cases}1, & upper\ bridge-arm\ on \\ 0, & lower\ bridge-arm\ on\end{cases} \tag{3}$$

Then (S_a, S_b, S_c) has eight combinations, including six non-zero vectors and two zero vectors. If taking (1, 0, 0) as an example, they have following constraints.

$$\begin{cases} U_a-U_b=U_{dc} \\ U_a-U_c=U_{dc} \\ U_a+U_b+U_c=0 \end{cases} \tag{4}$$

Solving (4), we can obtain that $U_a=2U_{dc}/3$, $U_b=-U_{dc}/3$, $U_c=-U_{dc}/3$. The relationship between the states of S_a, S_b, S_c and phase voltages are shown in Table I.

TABLE I
RELATIONSHIPS BETWEEN SWITCHING STATES AND PHASE VOLTAGES

Vector label	S_a S_b S_c	U_a	U_b	U_c	Vector expression
$\vec{U}_0$	000	0	0	0	0
$\vec{U}_4$	100	$\frac{2}{3}U_{dc}$	$-\frac{1}{3}U_{dc}$	$-\frac{1}{3}U_{dc}$	$\frac{2}{3}U_{dc}e^{0}$
$\vec{U}_6$	110	$\frac{1}{3}U_{dc}$	$\frac{1}{3}U_{dc}$	$-\frac{2}{3}U_{dc}$	$\frac{2}{3}U_{dc}e^{j\pi/3}$
$\vec{U}_2$	010	$-\frac{1}{3}U_{dc}$	$\frac{2}{3}U_{dc}$	$-\frac{1}{3}U_{dc}$	$\frac{2}{3}U_{dc}e^{j2\pi/3}$
$\vec{U}_3$	011	$-\frac{2}{3}U_{dc}$	$\frac{1}{3}U_{dc}$	$\frac{1}{3}U_{dc}$	$\frac{2}{3}U_{dc}e^{j\pi/3}$
$\vec{U}_1$	001	$-\frac{1}{3}U_{dc}$	$-\frac{1}{3}U_{dc}$	$\frac{2}{3}U_{dc}$	$\frac{2}{3}U_{dc}e^{j4\pi/3}$
$\vec{U}_5$	101	$\frac{1}{3}U_{dc}$	$-\frac{2}{3}U_{dc}$	$\frac{1}{3}U_{dc}$	$\frac{2}{3}U_{dc}e^{j5\pi/3}$
$\vec{U}_7$	111	0	0	0	0

This work is licensed under a Creative Commons Attribution 4.0 License. For more information, see https://creativecommons.org/licenses/by/4.0/.

This article has been accepted for publication in a future issue of this journal, but has not been fully edited. Content may change prior to final publication. Citation information: DOI 10.1109/ACCESS.2020.2993806, IEEE Access

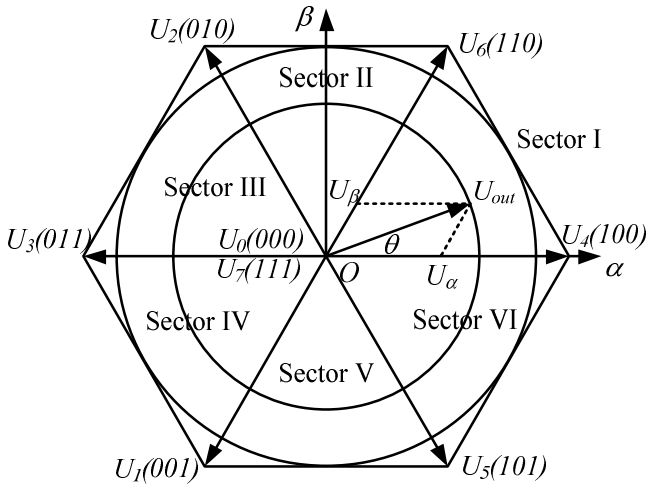

FIGURE 1. **Voltage space vector [21].**

Based on the results in Table 1, the magnitude and position of the eight voltage space vectors, as well as the division of the sectors are depicted in Fig. 1.

B. CONTROL ALGORITHM

1) SECTOR JUDGEMENT

First, the voltages U_α and U_β in the two-phase stationary coordinate system by Clarke transformation should be obtained. According to the geometric analysis of Fig. 1, it is easy to get the necessary and sufficient conditions falling in each sector, which are summarized as Table II.

2) SWITCHING TIME AND OVERMODULATION PROCESSING

Once the sector of a given voltage vector is determined, it can be known that which two non-zero vectors are to be combined, and then the switching time of the non-zero vector in one switching period is calculated. If there is remaining time, it is equally divided into two zero vectors. Taking the Sector I as an example, the active non-zero vectors are $\vec{U}_4$ and $\vec{U}_6$, and the given voltage vector decomposition in the $\alpha\beta$ coordinate system is shown in Fig. 2.

Applying average equivalence principle into Sector I:

$$\vec{U}_{ref}\cdot T_s=\vec{U}_4\cdot T_4+\vec{U}_6\cdot T_6 \tag{6}$$

$$\begin{bmatrix}U_\alpha\\U_\beta\end{bmatrix}T_s=U_{ref}\begin{bmatrix}\cos\theta\\\sin\theta\end{bmatrix}T_s=\frac{2}{3}U_{dc}\begin{bmatrix}1\\0\end{bmatrix}T_4+\frac{2}{3}U_{dc}\begin{bmatrix}\cos\frac{\pi}{3}\\\sin\frac{\pi}{3}\end{bmatrix}T_6 \tag{7}$$

$$\begin{cases}T_4=\dfrac{\sqrt{3}T_s}{U_{dc}}\left(\dfrac{\sqrt{3}}{2}U_\alpha-\dfrac{1}{2}U_\beta\right)\\T_6=\dfrac{\sqrt{3}T_s}{U_{dc}}U_\beta\\T_0=T_7=\dfrac{1}{2}(T_s-T_4-T_6)\end{cases} \tag{8}$$

TABLE II
THE JUDGING CONDITIONS FOR EACH SECTOR

Sector I	$U_\alpha>0$, $U_\beta>0$, and $U_\beta/U_\alpha<\sqrt{3}$
Sector II	$U_\alpha>0$ and $U_\beta/\lvert U_\alpha\rvert>\sqrt{3}$
Sector III	$U_\alpha<0$, $U_\beta>0$ and $-U_\beta/U_\alpha<\sqrt{3}$
Sector IV	$U_\alpha<0$, $U_\beta<0$ and $U_\beta/U_\alpha<\sqrt{3}$
Sector V	$U_\beta<0$ and $-U_\beta/\lvert U_\alpha\rvert>\sqrt{3}$
Sector VI	$U_\alpha>0$, $U_\beta<0$ and $-U_\beta/U_\alpha<\sqrt{3}$

Similarly, the vector switching time in other sectors can be calculated. Further, it can be found that there are three common factors in each vector switching time, represented by X, Y and Z, which can simplify the algorithm. The expression is as follows.

$$\begin{cases}X=\dfrac{\sqrt{3}T_s}{U_{dc}}U_\beta\\Y=\dfrac{\sqrt{3}T_s}{U_{dc}}\left(\dfrac{1}{2}U_\beta+\dfrac{\sqrt{3}}{2}U_\alpha\right)\\Z=\dfrac{\sqrt{3}T_s}{U_{dc}}\left(\dfrac{1}{2}U_\beta-\dfrac{\sqrt{3}}{2}U_\alpha\right)\end{cases} \tag{9}$$

Solving (9), we can get the results in Table III, where t_1 represents the switching time of the first active non-zero vector, t_2 represents the other one.

TABLE III
SWITCHING TIME OF NON-ZERO VECTORS

	Sector I	Sector II	Sector IIII	Sector IV	Sector V	Sector VI
t_1	$-Z$	Z	X	$-X$	$-Y$	Y
t_2	X	Y	$-Y$	Z	$-Z$	$-X$

When $t_1+t_2>T_s$, it needs to be overmodulated, otherwise the waveform will distort. The solution is shown as follows.

$$\begin{cases}t_1^*=\dfrac{t_1}{t_1+t_2}T_s\\t_2^*=\dfrac{t_2}{t_1+t_2}T_s\end{cases} \tag{10}$$

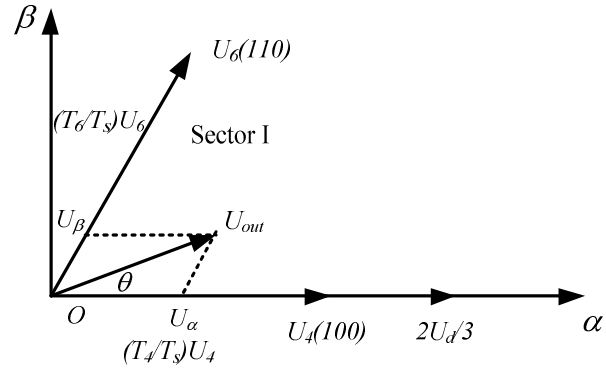

FIGURE 2. **Synthesis and decomposition of voltage space vector in Sector I.**

This work is licensed under a Creative Commons Attribution 4.0 License. For more information, see https://creativecommons.org/licenses/by/4.0/.

This article has been accepted for publication in a future issue of this journal, but has not been fully edited. Content may change prior to final publication. Citation information: DOI 10.1109/ACCESS.2020.2993806, IEEE Access

3) MODULATION RULES

The above steps have already obtained the switching time of the vector, the next question is how to generate the actual pulse width modulation waveform. In SVPWM modulation, the choice of zero vector has great flexibility. Reasonable selection and distribution of zero vector can greatly reduce the number of switching and switching losses [22]. Regardless of the modulation method, it should be based on the principle of switching state of one phase in each switching state transition, and the zero vector is evenly distributed in time, and the PWM waveform symmetry is kept as much as possible, which can reduce distortions and harmonics effectively.

III. PROPOSED SECTOR JUDGEMENT ALGORITHM

The innovation of the SVPWM algorithm proposed in this paper is to judge the sector where a predefined reference voltage vector is located, which reduces the calculation time of the SVPWM algorithm as a whole. The advantage is especially reflected in the fact that multiple inverters are connected in parallel leading to the number increasing of voltage vectors.

In the field of machine vision, robots are used to replace human eyes to make measurements and judgments. This paper is inspired by the fact that it can directly 'see' the sector in which the reference voltage vector is located, and the most important thing is that it can immediately give the switching time of two non-zero voltage vectors.

A. CONDUCT MATRIX

The reference voltage vector is analogized to the second hand on the clock, and then the vector plane formed by combining the six sectors is the dial. This paper constructs the 101-order matrix $\boldsymbol{s}$ as the 'dial' for the explanation, as shown in Fig.3.

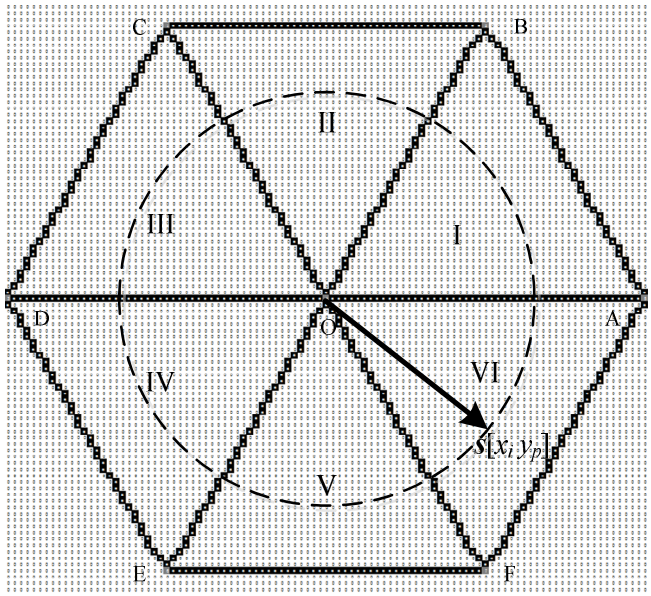

FIGURE 3. 101-order matrix as the 'dial'.

The vertex position of the regular hexagon, the edge (without vertexes), the elements at the boundary of the adjacent sector are filled with a specific number that is not zero, and the remaining elements are set to zero, ready for the algorithm. Each element of the matrix is equivalent to one pixel. When the endpoint of the composite vector falls on a certain pixel, the algorithm can quickly get which sector it locates. It should be noted here that the reference voltage vector has the meaning of amplitude and phase angle, and must be pre-processed before it is 'projected' into the sector formed by the matrix. According to the conventional SVPWM algorithm, each edge of the regular hexagon is equivalent to $2U_{dc}/3$, which is proportionally assigned to the row-column distance between matrix elements.

B. SELECT 'EDGE' HORIZONTALLY

Taking one sector as an example, assuming that the endpoint of the reference voltage vector falls at the position of $\boldsymbol{s}[x_i\ y_p]$ (Point O in Fig. 4), and $\boldsymbol{s}[x_i\ y_p] = 0$. Let $p\_f=p$, keep i unchanged, and then let $p\_f=p\_f+1$, until $\boldsymbol{s}[x_i\ y_{p\_f}]>10$, select the edge where $\boldsymbol{s}[x_i\ y_{p\_f}]$ is located now, which is point N; for the same reason, let $p\_b=p$, keep i unchanged, and then let $p\_b=p\_b-1$ until $\boldsymbol{s}[x_i\ y_{p\_b}]>10$, and then select the edge where $\boldsymbol{s}[x_i\ y_{p\_b}]$ is located now, which is point M. The two edges seen are the OF and AF in Fig. 4, respectively.

C. SECTOR JUDGEMENT

As can be seen from Fig. 3, each sector is a small equilateral triangle that can be uniquely determined by the three vertexes. On the basis of Section B, the forward selected edge defined as AF and the backward selected edge defined as OF can determine two vertexes respectively, and one of them isrepeated. Taking the forward selected edge as an example, the detailed process of how to find the position of two vertexes is explained as follows.

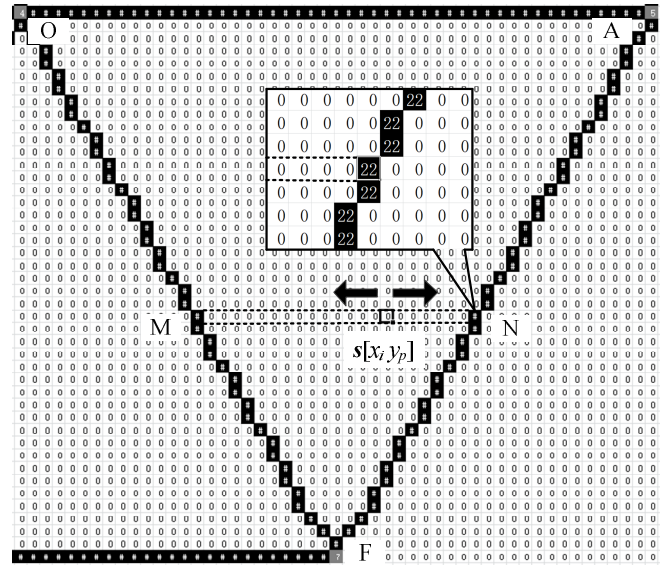

FIGURE 4. The selection process of the two edges of the sector.

This work is licensed under a Creative Commons Attribution 4.0 License. For more information, see https://creativecommons.org/licenses/by/4.0/.

This article has been accepted for publication in a future issue of this journal, but has not been fully edited. Content may change prior to final publication. Citation information: DOI 10.1109/ACCESS.2020.2993806, IEEE Access

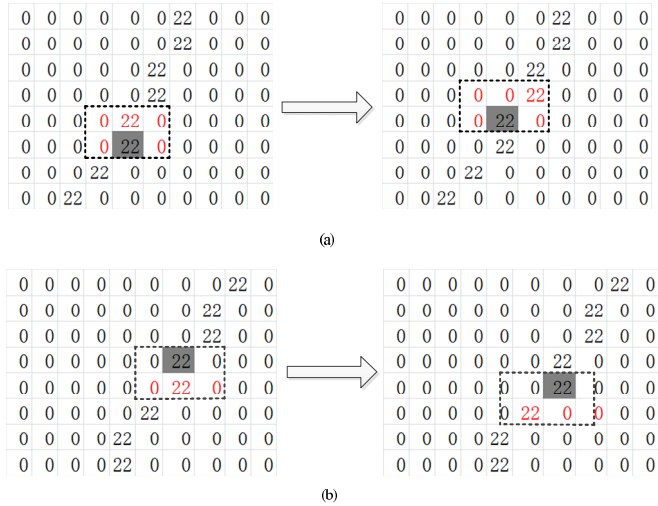

FIGURE 5. **The proposed method of how to find the vertexes of a sector. (a) Upward scanning. (b) Downward scanning.**

In Fig. 5(a), the zero elements in the $\boldsymbol{s}[x_i\ y_{p\_f-1}]$, $\boldsymbol{s}[x_i\ y_{p\_f+1}]$, $\boldsymbol{s}[x_{i-1}\ y_{p\_f-1}]$, $\boldsymbol{s}[x_{i-1}\ y_{p\_f}]$, and $\boldsymbol{s}[x_{i-1}\ y_{p\_f+1}]$ are replaced by 255 first. Then, judge which of the five elements is the smallest now, the corresponding position becomes the new $\boldsymbol{s}[x_i\ y_{p\_f}]$. By repeating the above process until the position of the first vertex is found upward. In the end, let s_1=$\boldsymbol{s}[x_i\ y_{p\_f}]$=5, which is the point A in Fig. 4.

Similarly, in Fig. 5(b), after replacing the zero elements by the figure 255 among $\boldsymbol{s}[x_{i+1}\ y_{p\_f-1}]$, $\boldsymbol{s}[x_{i+1}\ y_{p\_f}]$, and $\boldsymbol{s}[x_{i+1}\ y_{p\_f+1}]$, the three elements are compared to find the minimum one and the position of the minimum element becomes the new $\boldsymbol{s}[x_i\ y_{p\_f}]$. Also, by repeating the process above, the position of the second vertex downward will be found. Finally, let s_2=$\boldsymbol{s}[x_i\ y_{p\_f}]$=7, which is the point F in Fig. 4.

The way to find two vertexes of the selected backward edge is the same as above, through which point O and point F are determined. It should be noticed that point F is found twice, which is repeated. Besides, for the convenience of coding, the number filled in point O is set as 4.

At this point, the positions of the three vertexes can be uniquely determined, and the values of the three elements (s_1, s_2, s_3) will be used to determine the sector in which they are located.

IV. SIMULATIONS

To verify the proposed SVPWM algorithm, simulations are conducted using MATLAB/Simulink. The diagram of the whole system is shown as Fig. 6, the main difference between proposed method and conventional method is reflected in the sector judgment. Besides, the comparison on the output waveforms has been done between the proposed and conventional SVPWM.

Simulation conditions: Open loop, the voltage of DC side is 650V, adopting LC filtering while L=6mH, C=20μF.

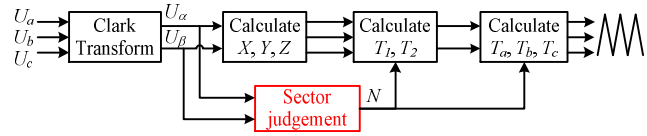

FIGURE 6. **The diagram of the whole system.**

A. SIMULATION RESULTS OF CONVENTIONAL SVPWM

The main purpose of this subsection is to verify that the proposed algorithm is feasible, so it is necessary to use the simulation results of conventional control algorithm as references. Phase voltages and line voltages are the most intuitive results that reflect the correctness of the algorithm.

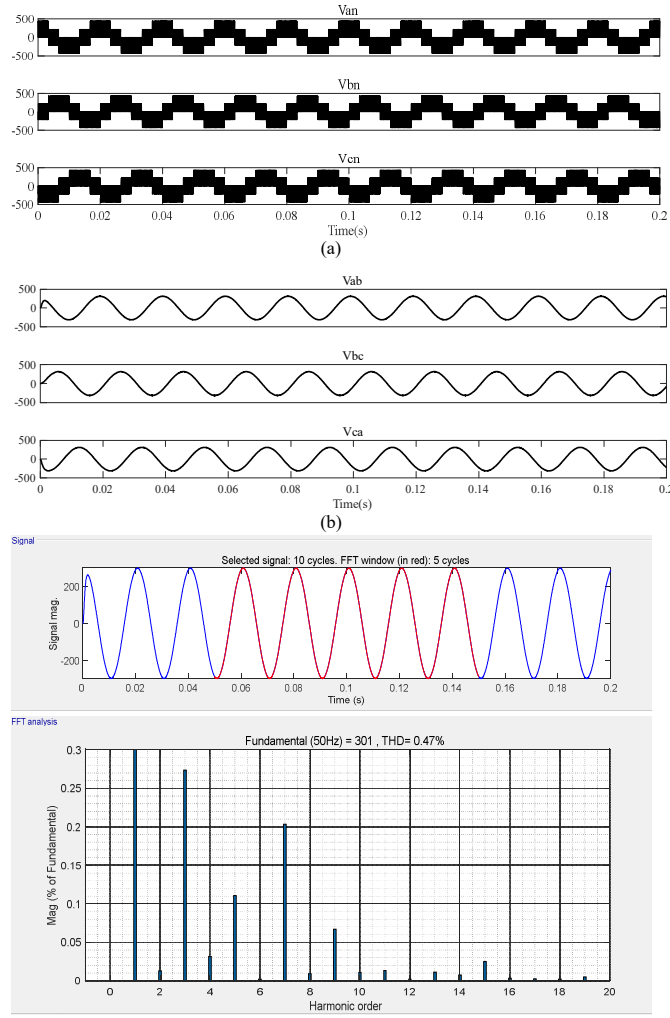

FIGURE 7. **Simulation results of conventional SVPWM. (a) Phase voltages. (b) Line voltages. (c) Total Harmonic Distortion.**

As shown in Figs. 7(a) and (b), the phase voltages have five levels such as $\pm 2U_{dc}/3$, $\pm 1U_{dc}/3$ and 0, while the line voltages are three-phase symmetric sinusoidal waves after LC filtering. Figs. 7(c) shows the THD of the line voltage modulated through conventional SVPWM, which is only 0.47%.

This work is licensed under a Creative Commons Attribution 4.0 License. For more information, see https://creativecommons.org/licenses/by/4.0/.

This article has been accepted for publication in a future issue of this journal, but has not been fully edited. Content may change prior to final publication. Citation information: DOI 10.1109/ACCESS.2020.2993806, IEEE Access

B. SIMULATION RESULTS OF PROPOSED SVPWM

In the case that the simulation topology and circuit parameters are unchanged, the waveforms of the proposed SVPWM are shown as Fig. 8. It can be seen from Fig. 8 that the proposed SVPWM algorithm is consistent with the conventional one in the effect of a single inverter, which validates the proposed SVPWM and makes it possible for the application in the multiple inverters connected in parallel.

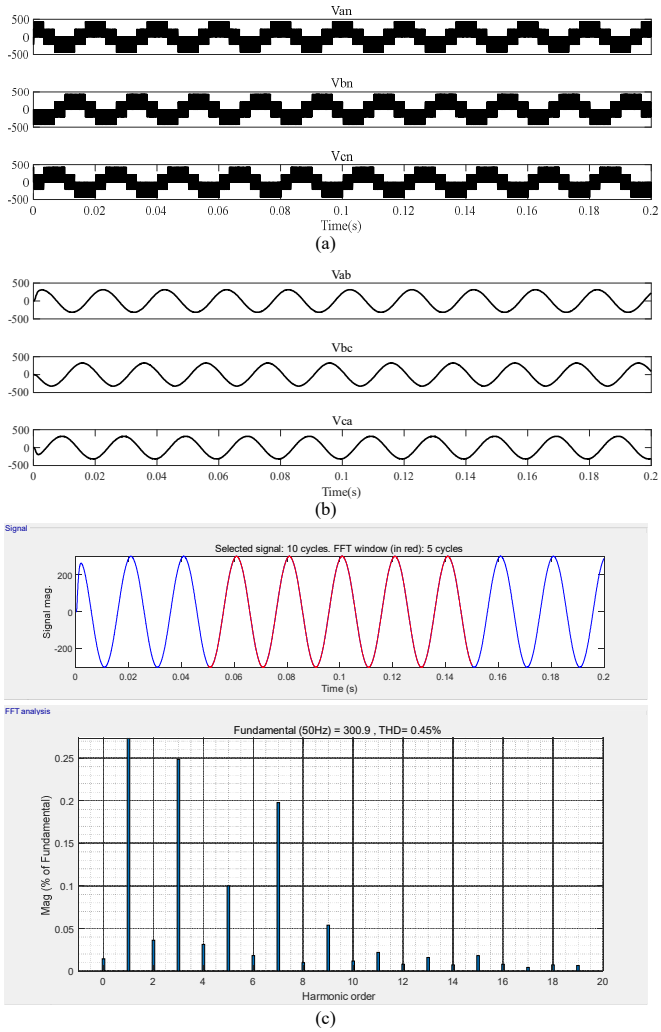

FIGURE 8. Simulation results of proposed SVPWM. (a) Phase voltages. (b) Line voltages. (c) Total Harmonic Distortion.

It shoul be notice that there is a variation in fundamental voltage in conventional method (301.0V) and proposed method (300.9V) which show in Figs. 7(c) and Figs. 8(c). The reason is that in proposed method sectors are formed by the elements of matrix, in the processing of determing which element exactly the predefined voltage vector fall on, it will sacrifice a little accuracy in exchange for a reduction in calculation time. The error will be eliminated in closed loop condition. Also, the erro caused that the pulse width of the control signal is slightly asymmetric. That is why the DC component appears in the output of the inverter. The DC component is within an acceptable range and can be eliminated by various methods.

C. EXECUTION TIME AND MEMORY UTILIZATION

In order to compare the advantages and disadvantages of the two methods more specifically, the execution time and memory utilization are discussed in this section. Fig. 9(a) and (b) show the execution time of two methods.

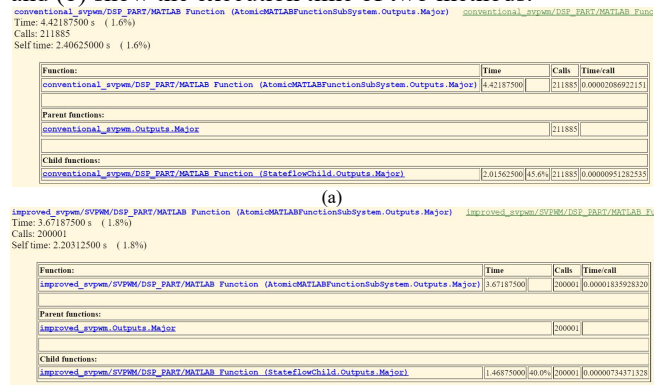

FIGURE 9. Execution time. (a) Conventional algorithm. (b) Proposed algorithm.

Under the same conditions, the total execution time of the conventional and proposed methods are 268.11s and 207.41s, where the time of sector judgement are 4.421875s and 3.671875s, respectively. The results show that the proposed algorithm is better in execution time.

Fig. 10 (a) and (b) show the memory utilization of two methods. Due to the existence of large-dimensional matrix, the proposed algorithm is slightly inferior to the conventional algorithms in memory utilization, but they are very close. In general, the proposed algorithm has more advantages in execution time when the memory utilization is equivalent.

```
Physical Memory (RAM):
    In Use:                  5225 MB (  1469b6000)
    Free:                    6961 MB (  1b31b0000)
    Total:                  12187 MB (  2f9b66000)
Page File (Swap space):
    In Use:                  5241 MB (  147977000)
    Free:                   19233 MB (  4b21ef000)
    Total:                  24475 MB (  5f9b66000)
Virtual Memory (Address Space):
    In Use:                 15593 MB (  3ce960000)
    Free:                  134202134 MB (7ffc31680000)
    Total:                 134217727 MB (7fffffff0000)
```

(a)

```
Physical Memory (RAM):
    In Use:                  5246 MB (  147eda000)
    Free:                    6940 MB (  1b1c8c000)
    Total:                  12187 MB (  2f9b66000)
Page File (Swap space):
    In Use:                  5295 MB (  14af15000)
    Free:                   19180 MB (  4aec51000)
    Total:                  24475 MB (  5f9b66000)
Virtual Memory (Address Space):
    In Use:                 15784 MB (  3da8fe000)
    Free:                  134201942 MB (7ffc256e2000)
    Total:                 134217727 MB (7fffffff0000)
```

(b)

FIGURE 10. Memory utilization. (a) Conventional algorithm. (b) Proposed algorithm.

This work is licensed under a Creative Commons Attribution 4.0 License. For more information, see https://creativecommons.org/licenses/by/4.0/.

This article has been accepted for publication in a future issue of this journal, but has not been fully edited. Content may change prior to final publication. Citation information: DOI 10.1109/ACCESS.2020.2993806, IEEE Access

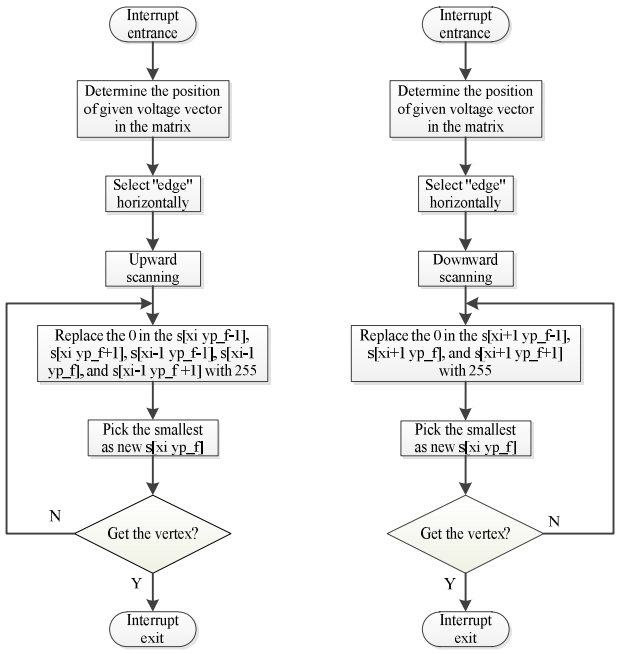

FIGURE 11. **Program flow chart of how to find the vertexes of a sector. (a) Upward scanning. (b) Downward scanning.**

V. EXPERIMENTS

To double check the effectiveness of the proposed SVPWM algorithm, an experimental setup has been built and experiments have been carried out in the laboratory, as shown in Fig. 12. The control signals are given by digital signal processor (DSP) with the type of TMS320F28335 to drive a three-phase inverter. Parameters of the experimental setup are listed in Table IV.

The program flow charts of two sector judgement methods are shown in the Figs. 11 and Fig. 13. Fig. 11 shows the proposed method, where the three vertexes of the sector are obtained through upward and downward scanning and then sectors can be uniquely determined. Fig. 13 shows the conventional method, where the sector is distinguished by geometric relationship.

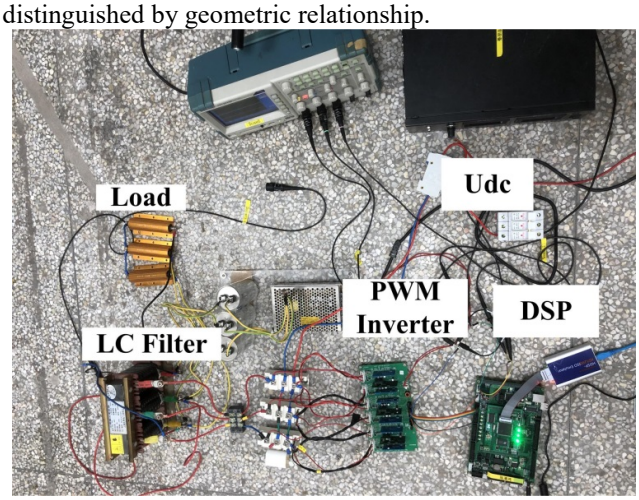

FIGURE 12. **Experimental setup.**

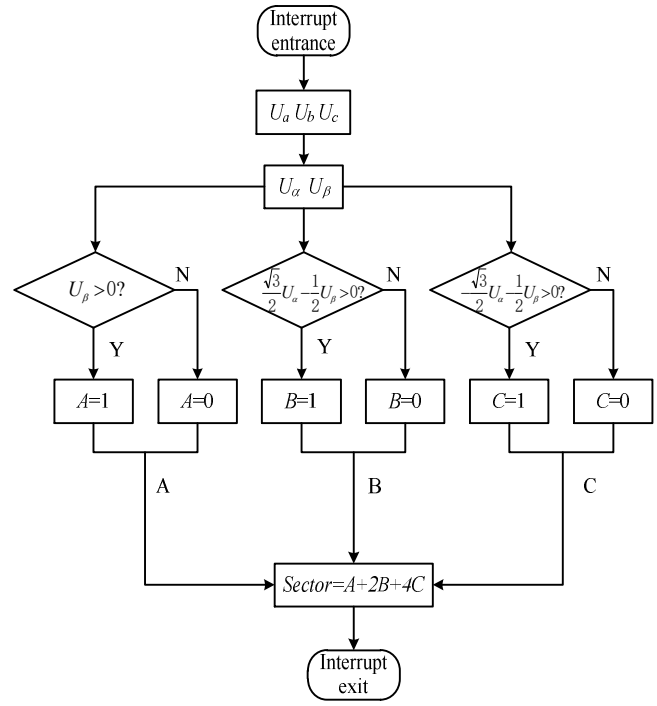

FIGURE 13. **Program flow chart of conventional sector judgement.**

TABLE IV
PARAMETERS FOR EXPERIMENTS

Items	Values
U_{dc}	50V
Inductance of filter (L)	5mH
Capacitance of filter (C)	30μF
Load	50Ω
Switching frequency	5kHz

In the proposed algorithm, the sector is judged based on the sum of the numbers on the three vertexes of the equilateral triangle. Sector I to VI correspond to the case of s=11, 7, 8, 13, 17, 16, as shown in the Fig. 14. Take Sector I as an example, if the given voltage is located in it, the values of three vertexes are 4, 2 and 5 respectively, and then s=4+2+5=11.

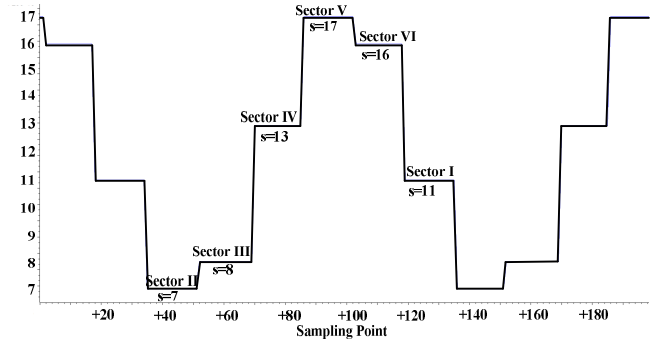

FIGURE 14. **The settings of correspondence of Sectors.**

The experimental waveforms of three-phase phase voltages and line voltages are shown in the Fig. 15, where

This work is licensed under a Creative Commons Attribution 4.0 License. For more information, see https://creativecommons.org/licenses/by/4.0/.

This article has been accepted for publication in a future issue of this journal, but has not been fully edited. Content may change prior to final publication. Citation information: DOI 10.1109/ACCESS.2020.2993806, IEEE Access

three channels are recorded as Phase A, B and C respectively. It can be seen that three-phase voltages are 120° out of each other with good symmetry, which has validated the proposed control algorithm.

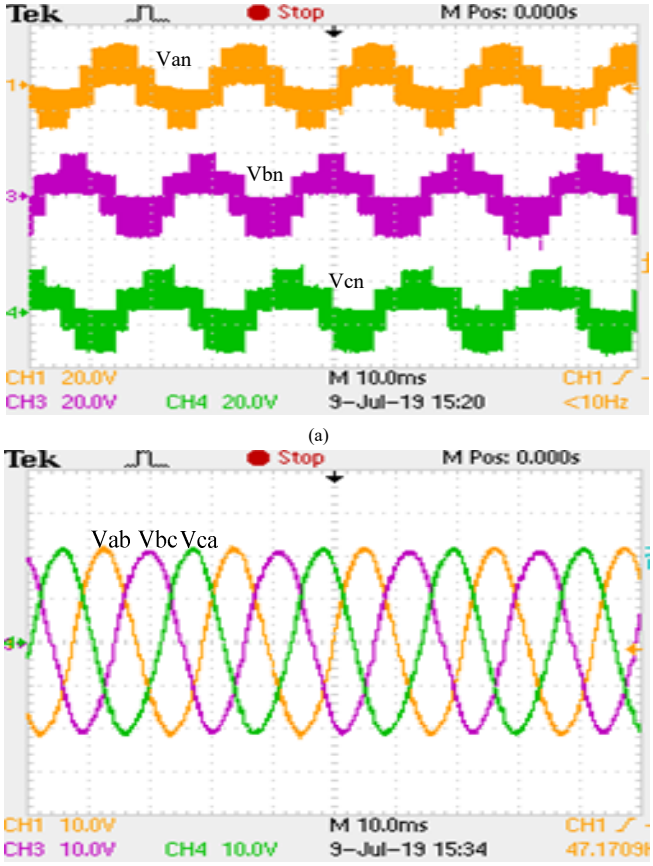

FIGURE 15. Experimental waveforms of the proposed SVPWM. (a) Phase voltages. (b) Line voltages.

VI. CONCLUSIONS

This paper proposes a novel method simulating human eye recognition for sector judgement of SVPWM Algorithm. The innovation is to judge the sector where a predefined voltage vector is located, the process of which is like human eye recognition that can greatly reduce the whole calculation time of the SVPWM algorithm. It is believed that the advantage will become more obvious as the number of voltage vectors is multiplied, especially in the application of multiple inverters or multilevel inverters. In the case study, machine vision is used to replace human eyes to judge the sector where the voltage vectors locate. The detailed design process and program flow charts are well illustrated. The feasibility of the proposed SVPWM algorithm has been validated by both simulation and experimental results. Finally, it has been verified in two-level inverter that the proposed algorithm has more advantages in execution time when the memory utilization is equivalent.

VII. ACKNOWLEDGMENTS

This work was supported by the Natural Science Foundation of Jiangsu Province under project BK20170675, and by the National Natural Science Foundation of China under project 51877040.

REFERENCES

[1] S. Dusmez, L. Qin, and B. Akin, "A New SVPWM Technique for DC Negative Rail Current Sensing at Low Speeds", *IEEE Trans. Ind. Electron.*, vol. 62, no. 2, pp. 826-831, Jul. 2015.

[2] Z. Gong, X. Wu, P. Dai, and R. Zhu, "Modulated model predictive control for MMC-based active front-end rectifiers under unbalanced grid conditions," *IEEE Trans. Ind. Electron.*, vol. 66, no. 3, pp. 2398–2409, Mar. 2019.

[3] K. Zhang, Y. Kang, J. Xiong, and J. Chen, "Direct repetitive control of SPWM inverter for UPS purpose", *IEEE Trans. Power Electron.*, vol. 18, no. 3, pp. 784-792, May. 2003.

[4] C. Xie, X. Zhao, K. Li, et al., "Multirate resonant controllers for grid-connected inverters with harmonic compensation function", *IEEE Trans. Power Electron.*, vol. 66, no. 99, pp. 8981–8991, Nov. 2018.

[5] Y. Liang, C. O. Nwankpa, "A new type of STATCOM based on cascading voltage-source inverters with phase-shifted unipolar SPWM", *IEEE Trans. Ind. Appli.*, vol. 35, no. 5, pp. 1118–1123, Sep. 1999.

[6] H. W. Van der Broeck, H.C. Skldelny, and G.V. Stanke, "Analysis and realization of a pulse-width modulator based on voltage space vectors", *IEEE Trans. Ind. Appl.*, vol. 24, no. 1, pp. 142–150, Jan. 2008.

[7] M. Kumar, R. Gupta, "Sampling effect characterization of digital SPWM of VSI in time domain", *IEEE Trans. Ind. Electron.*, vol. 63, no. 7, pp. 4150-4159, 2016.

[8] M. Kumar, R. Gupta, "Time-domain characterisation of multicarrier-based digital SPWM of multilevel VSI", *IET Power Electron.*, vol. 11, no. 1, pp. 100-109, Jan. 2018.

[9] G. H. Liu, L. Qu, W. X. Zhao, et al., "Comparison of two SVPWM control strategies of five-phase fault-tolerant permanent-magnet motor", *IEEE Trans. Power Electron.*, vol. 31, no. 9, pp. 6621-6630, 2016.

[10] H. F. Bai, J. W. Zhu, J. H. Sun, et al., "Comparative study of different fault-tolerant control strategies for dual-winding fault tolerant permanent magnet motor", *Trans. China Electrotech. Soc.*, vol. 31, no. 13, pp. 189-199, 2016.

[11] C. Wang, K. Wang, and X. You, "Research on Synchronized SVPWM Strategies Under Low Switching Frequency for Six-Phase VSI-Fed Asymmetrical Dual Stator Induction Machine", *IEEE Trans. Ind. Electron.*, vol. 63, no. 11, pp. 6767-6776, Nov. 2016.

[12] V. Vlatkovic, "Digital-signal-processor-based control of three phase space vector modulated converters", *IEEE Trans. Ind. Electron.*, vol. 41, no. 3, pp. 326–332, Jun. 1994.

[13] E. Levi, R. Bojoi, F. Profumo, H. A. Toliyat, and S. Williamson, "Multiphase induction motor drives-a technology status review", *IET Elect. Power Appl.*, vol. 1, no. 4, pp. 489–516, July. 2007.

[14] L. Parsa, H. A. Toliyat, "Fault-tolerant interior-permanent-magnet machines for hybrid electric vehicle applications", *IEEE Trans. Veh. Technol.*, vol. 56, no. 4, pp. 1546-1552, Jul. 2007.

[15] Q. Wang, M. Cheng, Y. Jiang, W. Zuo, and G. Buja, "A simple active and reactive power control for applications of single-phase electric springs", *IEEE Trans. Ind. Electron.*, vol. 65, no. 8, pp. 6291-6300, Aug. 2018.

[16] Z. Liu, Y. Wang, G. Tan, et al., "A novel SVPWM algorithm for five-level active neutral-point-clamped converter", *IEEE Trans. Power Electron.*, vol. 31, no. 5, pp. 3859-3866, Jul. 2016.

[17] X. Li, S. Dusmez, B. Akin, K. Rajashekara, "A new SVPWM for the phase current reconstruction of three-phase three-level T-type converters", *IEEE Trans. Power Electron.*, vol. 31, no. 3, pp. 2627-2637, Mar. 2016.

[18] O. C. Kivanc, S. B. Ozturk, "Sector determination for SVPWM based four-switch three-phase VSI", *Electron. Lett.*, vol. 53, no. 5, pp. 343-345, Mar. 2017.

This work is licensed under a Creative Commons Attribution 4.0 License. For more information, see https://creativecommons.org/licenses/by/4.0/.

This article has been accepted for publication in a future issue of this journal, but has not been fully edited. Content may change prior to final publication. Citation information: DOI 10.1109/ACCESS.2020.2993806, IEEE Access

[19] Z. Wang, Y. Wang, J. Chen, and M. Chen, "Fault tolerant control of NPC three-level inverters fed double-stator-winding PMSM drives based on vector space decomposition", *IEEE Trans. Ind. Electron.*, vol. 64, no. 11, pp. 8446-8458, May 2017.
[20] M. Schaefer, W. Goetze, M. Hofmann, F. Bayer, et al., "Direct current control for grid-connected diode-clamped inverters", *IEEE Trans. Ind. Electron.*, vol. 64, no. 4, pp. 3067-3074, Apr. 2017.
[21] D. W. Chung, J. S. Kim, and S. K. Sul, "Unified Voltage Modulation Technique for Real-Time Three-Phase Power Conversion", *IEEE Trans. Ind. Applicat.*, Vol.34, pp374-380, March/April 1998.
[22] R. S. Kanchan, M. R. Baiju, K. K. Mohapatra, P. P. Ouseph and K. Gopakumar, "Space vector PWM signal generation for multilevel inverters using only the sampled amplitudes of reference phase voltages", *IEE Proceedings - Electric Power Applications*, vol. 152, no. 2, pp. 297-309, 4 March 2005.

Qingsong Wang (S'14-M'17-SM'17) received the B.Sc. and M.Sc. degrees from the Department of Electrical Engineering, Zhejiang University, Hangzhou, China, in 2004 and 2007, respectively, and the Ph.D. degree from the School of Electrical Engineering, Southeast University, Nanjing, China, in 2016. From November 2015 to November 2016, he was a joint Ph. D student with the Department of Energy Technology, Aalborg University, Aalborg, Denmark, where he focused on electric springs.
From July 2004 to July 2005, he was an engineer in Shihlin Electronic & Engineering Co., Ltd, Suzhou, China. From July 2007 to August 2011, he was an engineer in Global Development Center of Philips Lighting Electronics, Shanghai, China. In October 2010, he was promoted to be a Senior Engineer. From August 2011 to September 2013, he was a Lecturer in PLA University of Science and Technology, Nanjing, China. Since 2017, he has been with Southeast University, where he is currently a Lecturer in the School of Electrical Engineering. He is also with Jiangsu Key Laboratory of Smart Grid Technology and Equipment.
Dr. Wang's research interests are focused in the areas of control and applications of power electronics to power systems.

Panhong Chen received the B.Sc. degree in electrical engineering from China University of Mining and Technology, Xuzhou, China, in 2018. He is currently working toward the M.Sc. degree with the School of Electrical Engineering, Southeast University, Nanjing, working on the control of electric springs.
His current research interests include applications of power electronics to power systems.

Fujin Deng (S'10-M'13) received the B.Eng. degree in electrical engineering from China University of Mining and Technology, Jiangsu, China, in 2005, the M.Sc. Degree in electrical engineering from Shanghai Jiao Tong University, Shanghai, China, in 2008, and the Ph.D. degree in energy technology from the Department of Energy Technology, Aalborg University, Aalborg, Denmark, in 2012. He joined the Southeast University in 2017 and is currently a Professor in the School of Electrical Engineering, Southeast University, Nanjing, China. From 2013 to 2015 and from 2015 to 2017, he was a Postdoctoral Researcher and an Assistant Professor, respectively, in the Department of Energy Technology, Aalborg University, Aalborg, Denmark. His main research interests include wind power generation, multilevel converters, high-voltage direct-current (HVDC) technology, DC grid, and offshore wind farm-power systems dynamics.

Ming Cheng (M'01–SM'02–F'15) received the B.Sc. and M.Sc. degrees from the Department of Electrical Engineering, Southeast University, Nanjing, China, in 1982 and 1987, respectively, and the Ph.D. degree from the Department of Electrical and Electronic Engineering, The University of Hong Kong, Hong Kong, in 2001.
Since 1987, he has been with Southeast University, where he is currently a Professor in the School of Electrical Engineering and the Director of the Research Center for Wind Power Generation. His teaching and research interests include electrical machines, motor drives for electric vehicles, and renewable energy generation. He has authored or coauthored over 300 technical papers and four books and is the holder of 55 patents in these areas.
Prof. Cheng is a fellow of the Institution of Engineering and Technology (IET). He has served as chair and organizing committee member for many international conferences. He is a Distinguished Lecturer of the IEEE Industry Applications Society (IAS) in 2015/2016.

Giuseppe Buja (M'75–SM'84–F'95–LF'13) received the 'Laurea' degree with honors in power electronics engineering from the University of Padova, Padova, Italy, where he is currently a Full Professor. He has carried out an extensive research work in the field of power and industrial electronics, originating the modulating-wave distortion and the optimum modulation for pulse-width modulation inverters, pioneering the introduction of digital signal processing in the control systems of power electronics converters, and conceiving advanced techniques for the control of electric drives. His current research interests are automotive electrification, including wireless charging of electric vehicles, and grid-integration of renewable energies.
Dr. Buja received the IEEE Industrial Electronics Society (IES) Eugene Mittelmann Achievement Award "in recognition of his outstanding technical contributions to the field of industrial electronics," and the 2016 Best Paper Award from the IEEE Transactions on Industrial Electronics. He has served the IEEE in several capacities, including as General Chairman of the 20th Annual Conference of the IES (IECON) in 1994. Currently, he is an Associate Editor of the IEEE Transactions on Industrial Electronics, a Member of the Editorial Board of the *Chinese Journal of Electrical Engineering*, and a Senior Member of the Administrative Committee of the IES.

This work is licensed under a Creative Commons Attribution 4.0 License. For more information, see https://creativecommons.org/licenses/by/4.0/.